

Low-dimensional quantum antiferromagnetic Heisenberg model studied using Wigner-Jordan transformations

Y. R. Wang

Xerox Webster Research Center, 800 Phillips Road, 0114-41D, Webster, New York 14580

(Received 26 June 1991; revised manuscript received 13 January 1992)

A Wigner-Jordan (WJ) transformation is used to study the one-dimensional (1D) and two-dimensional (2D) quantum antiferromagnetic Heisenberg model. The advantage of using the Wigner-Jordan transformation is that it preserves all spin-commutation relations as well as the spin on-site exclusion principle. In the 1D case a nearest-neighbor covalent-bonding state of the WJ fermions is found to have a ground-state energy ($-0.4351J$ per site) comparable with that from the Bethe-ansatz solution ($-0.4431J$ per site), and a linear energy spectrum at low energies with velocity $1.6366J$, in close agreement with the velocity obtained by Haldane for the quantum antiferromagnetic Heisenberg model with $1/d^2$ interaction ($1.5708J$). The method used for studying the 1D model is then applied to the 2D Heisenberg model in a square lattice. The resulting state at finite temperature is the in-phase flux state, i.e., a flux state of the Wigner-Jordan spinless fermions with an in-phase fermion orbital current circulating around each elementary plaquette. The single-particle excitation spectrum, i.e., the energy dispersion of reversing orientation of a spin in the system, of the in-phase flux state is overall similar to that of spin waves, with significant difference near the edge point $\mathbf{k}=(\pi,0)$, at which the excitation energy of the WJ fermion is zero, whereas that of the spin-wave excitation is $2J$. The specific heat of the in-phase flux state predicts a correct temperature dependence over the entire temperature range, namely a T^2 dependence at low temperature, a peak near $T/J=0.6$, and a $1/T^2$ decreasing at high temperature. It also gives excellent agreement with the specific heat calculated from numerical methods. In contrast, the spin-wave theory only correctly predicts a T^2 dependence at low temperature. The Raman spectrum of the in-phase flux state is calculated and shows significant improvement over that from spin-wave theories compared with the experimental spectrum of La_2CuO_4 . The exchange parameter, J , obtained from the comparison is 1060 cm^{-1} , in agreement with that obtained from analyzing the neutron-scattering data.

I. INTRODUCTION

Quantum antiferromagnetism is a well-studied subject, but many important issues remain unresolved. The subject becomes particularly pressing because of the discovery of the high-temperature copper oxide superconductors. The undoped copper oxide materials, such as La_2CuO_4 , are layered antiferromagnets with local spin moments $S=\frac{1}{2}$. It is generally believed that the antiferromagnetic (AFM) behavior of the high- T_c materials can be modeled rather well by the $S=\frac{1}{2}$ two-dimensional (2D) AFM Heisenberg model. Neutron-scattering¹⁻³ and Raman-scattering⁴⁻⁷ experiments indicate that the intralayer nearest-neighbor exchange parameter is on the order of 1000 K, whereas that of the interlayer coupling is about 5 orders of magnitude smaller.⁸ While the small interlayer coupling is believed responsible for the three-dimensional (3D) AFM ordering of the spins in La_2CuO_4 , the temperature range for the interlayer coupling to have a major effect is expected to be extremely narrow.

The dimensionality plays an important role in studying the quantum ($S=\frac{1}{2}$) Heisenberg antiferromagnet. In one dimension (1D), the Heisenberg model can be solved exactly using the Bethe ansatz.^{9,10} The solution is a liquid of spin-singlet pairs. In three dimensions, the spins can be ordered antiferromagnetically below the Néel temperature, and spin-wave theory¹¹ is generally accepted as a

proper representation of the excitation spectrum at low temperatures. The situation in 2D is much less clear. While an antiferromagnetic ordering at $T=0$ for the quantum AFM Heisenberg model in a square lattice is found by many investigators^{8,12-14}, a true long-range AFM order at finite temperature cannot exist according to the Mermin-Wagner theorem.¹⁵ Quantum spins obey¹⁶ an on-site "exclusion principle," i.e. $S_i^+ S_i^- + S_i^- S_i^+ \equiv 1$, at any site i , where S_i^+ and S_i^- are the spin raising and lowering operators, respectively. This identity is a unique property of the quantum spins. Any successful theory has to at least approximately preserve it. When the spin operators are represented by boson operators, such as through the Holstein-Primakoff transformation,¹⁷ the identity states that the bosons can only singly occupy a lattice site. The spin-wave theory for the 3D Heisenberg AFM model indeed has a very small probability for the bosons more than singly occupying a lattice site, but the probability for the 2D spin-wave theory is too large to preserve the identity.¹⁶

In this work we use an extended Wigner-Jordan (WJ) transformation to study the 2D AFM $S=\frac{1}{2}$ Heisenberg model. Some of the results have been briefly reported in our previous rapid communications.^{18,19} The advantage of using the Wigner-Jordan transformation is that it automatically preserves all spin commutation relations, as well as the spin on-site exclusion principle mentioned

above. In contrast, the Holstein-Primakoff transformation, for example, only preserves the spin-commutation relations. Infinite repulsive interactions at every lattice site have to be added to the Holstein-Primakoff transformation in order to preserve the spin on-site exclusion principle.¹⁶ A detailed description of the WJ transformation will be given in Sec. II. In Sec. III, we show that the 1D quantum AFM Heisenberg model can be described as a liquid of interacting WJ fermions. A nearest-neighbor covalent bonding state of the WJ fermions is shown to have a correct excitation spectrum and a good ground-state energy compared with that of the exact Bethe-ansatz solution.^{9,10} In Sec. IV, we study the 2D AFM Heisenberg model in a square lattice using a method similar to that used for the 1D case. The 2D Heisenberg model can be viewed as, in the mean-field sense, a liquid of interacting WJ fermions moving in a self-generated gauge field. The resulting state, with a linear dispersion spectrum at small excitation energy and no true long-range AFM order at finite temperature, is the in-phase flux state. The single-particle excitation spectrum of the in-phase flux state is overall similar to that of spin waves, but significant differences exist and therefore could be examined by neutron-scattering experiments. The specific heat of the in-phase flux state predicts a correct temperature dependence over the entire temperature range, and gives excellent agreement with that calculated from numerical methods. In Sec. V, we present the calculation of the Raman spectrum of the in-phase flux state and show that it agrees very well with the experimental spectrum of La_2CuO_4 . A summary and discussion will be given in Sec. VI.

II. THE 2D WIGNER-JORDAN TRANSFORMATION

The original WJ transformation²⁰ transforms the 1D $S = \frac{1}{2}$ spin operators into spinless fermion operators. The 2D extension of the transformation has been discussed by several authors.^{18,19,21-23} Here we follow the method given in our previous reports.^{18,19} Using the original 1D transformation as a guideline,^{20,24} we define a spinless fermion annihilation operator, d_i , at site i , by

$$d_i = e^{-i\varphi_i} S_i^-, \quad (1)$$

and assume the phase, φ_i , to be of the form $\varphi_i = \sum_{j \neq i} d_j^\dagger d_j B_{ij}$, where B_{ij} is a c -number matrix element. It is immediately observable that φ_i commute with d_i , and hence with S_i^- , and that $[\varphi_i, \varphi_j] = 0$ for any site i and j . The spin on-site exclusion principle mentioned in the Introduction is automatically satisfied since the d_i 's are assumed to be fermion operators. The matrix element B_{ij} can be determined by the spin-commutation relation, $[S_i^+, S_j^-] = 0$, for any site $j \neq i$. Substituting Eq. (1) into the commutation relation and noticing the following identity:

$$e^{-i\varphi_i} d_j e^{i\varphi_i} = e^{iB_{ij}} d_j, \quad (2)$$

we obtain the equation for determining B_{ij} to be $e^{iB_{ij}} = -e^{iB_{ji}}$. Obviously the relative angles of the 2D

spin coordinates satisfy this equation. We therefore have $B_{ij} = \text{Im} \ln(\tau_j - \tau_i)$, and

$$\varphi_i = \sum_{j \neq i} d_j^\dagger d_j \text{Im} \ln(\tau_j - \tau_i), \quad (3)$$

where $\tau_j = x_j + iy_j$ is the complex coordinate of the j th spin. Finally, since $S_i^+ S_i^- = S^2 - S_i^z + S_i^z$, we have

$$S_i^z = d_i^\dagger d_i - \frac{1}{2}. \quad (4)$$

Equations (1), (3), and (4) constitute the complete 2D WJ transformation. The transformation is exact since all the other spin-commutation relations, such as $[S_i^z, S_j^\pm] = S_i^\pm \delta_{ij}$, are also satisfied by the transformation. It is also worthwhile to notice that the choice of the phase in Eq. (3) is not unique. There is a local gauge invariance, namely, that one could replace φ_i by $\varphi_i + C_i$, where C_i is any c number. This gauge invariance will be explicitly seen when we later express the phase factor in terms of a vector potential [cf., Eq. (16) below].

There are two intrinsic properties of this WJ representation of quantum spins with antiferromagnetic interaction. First, by summing over all the spin sites, we have $\sum_i d_i^\dagger d_i = N/2 + \sum_i S_i^z$. Since $\sum_i \langle S_i^z \rangle = 0$ for an antiferromagnetically ordered or a paramagnetic (disordered) spin state, the thermally averaged number of WJ fermions for the two cases is always half of the total spin sites. Since there are N states available for the WJ fermions, they fill exactly half of the total states at $T=0$. We therefore can speak of the spectrum of WJ fermions as consisting of a particle band, referring to the unfilled half of the total states, and a hole band, referring to the filled half of the total states. Second, let us start with a state which satisfies $\sum_i S_i^z = 0$, and then flip one spin from down to up, so that now $\sum_i S_i^z = 1$. Accordingly we have $\sum_i d_i^\dagger d_i = N/2 + 1$, meaning that one WJ fermion is added to the system. We can carry the same process of flipping a spin from up to down, and show that it corresponds to subtracting a WJ fermion from the system. The two processes must have the same excitation energy if the spins are interacting through the Heisenberg Hamiltonian. We thus can assert that the energy spectrum of the WJ fermions must possess a particle-hole symmetry. In the following sections we shall see that these two properties are observed by our mean-field solutions.

The transformation in Eqs. (1), (3), and (4) could take a slightly different form for the case of a bipartite lattice. In this case we can define two kinds of fermion annihilation operators, A_i and B_j , for sublattices A and B , respectively. For sublattice A , we define A_i 's to be the same as that given in the above equations, i.e.,

$$S_i^- = e^{i\varphi_i} A_i, \quad S_i^z = A_i^\dagger A_i - \frac{1}{2}, \quad (5)$$

with

$$\varphi_i = \sum_{l \neq i} A_l^\dagger A_l B_{il} + \sum_m (1 - B_m^\dagger B_m) B_{im}, \quad (6)$$

whereas for sublattice B we make a particle-hole transformation, i.e.,

$$S_j^- = e^{i\varphi_j} B_j^\dagger, \quad S_j^z = \frac{1}{2} - B_j^\dagger B_j, \quad (7)$$

with

$$\varphi_j = \sum_{m \neq j} (1 - B_m^\dagger B_m) B_{jm} + \sum_l A_l^\dagger A_l B_{jl} . \quad (8)$$

The advantage of this transformation is that the number of operators, $A_i^\dagger A_i$ and $B_j^\dagger B_j$, now can be interpreted as the deviation from the maximum antiferromagnetically ordered value, and therefore A_i^\dagger 's and B_j^\dagger 's are the excitations of the antiferromagnetically ordered state (i.e., the Néel vacuum).

III. ONE-DIMENSIONAL AFM HEISENBERG MODEL

In this section we study the $S = \frac{1}{2}$ 1D AFM Heisenberg model using the WJ transformation. Since there is an exact solution from the Bethe ansatz in this case, our results can be compared, and the approximation techniques can be examined.

The 1D WJ transformation can be viewed as a special case of our 2D transformation with the replacement of B_{ij} by either 0 or π in all the equations in the above section, since the relative angle between two spin sites in a 1D chain can only be one of the two values. The Heisenberg Hamiltonian, $H = J \sum_i S_i \cdot S_{i+1}$, is transformed into the one given below

$$H = J \sum_i d_i^\dagger d_{i+1} + J \sum_i (d_i^\dagger d_i - \frac{1}{2})(d_{i+1}^\dagger d_{i+1} - \frac{1}{2}) . \quad (9)$$

The first term of Eq. (9) comes from the XY part of the spin Hamiltonian, whereas the second term corresponds to the Ising part. The phase factor disappears from the Hamiltonian because $e^{i(\varphi_{i+1} - \varphi_i)} = e^{i\pi d_i^\dagger d_i}$ does not have any effect when operating before d_i^\dagger . It is immediately obvious from Eq. (9) that the 1D $S = \frac{1}{2}$ Heisenberg model corresponds to the 1D gas of interacting WJ spinless fermions.

We next study Eq. (9) using a mean-field theory with proper inclusion of second-order corrections. The Hamiltonian is separated into a mean-field part, H_{MF} , and a fluctuation part, H_1 , i.e., $H = H_{\text{MF}} + H_1$, where

$$H_{\text{MF}} = J \sum_i d_i^\dagger d_{i+1} + J \sum_i (2\Delta) d_i^\dagger d_{i+1} + NJ\Delta^2 , \quad (10)$$

and N is the total number of lattice sites. $\Delta = \langle d_i d_{i+1}^\dagger \rangle$ is the mean field. This definition of Δ implies a nearest-neighbor ‘‘covalent bonding’’ of the WJ fermions, analogous to the chemical bonding of the electrons. We shall call the resulting state of Eq. (10) the nearest-neighbor covalent-bonding state of the WJ fermions because of this analogy. It is easy to see that the single-particle energy of momentum k from Eq. (10) is

$$E_k = J(1 + 2\Delta)\cos k , \quad (11)$$

and that the self-consistent solution of Δ is

$$\Delta = -\frac{1}{N} \sum_k n_F(E_k) \cos k , \quad (12)$$

where $n_F(E_k)$ is the Fermi function of energy E_k . (We use the units $\hbar = k_B = a = 1$ throughout this paper, where

a is the lattice constant.) The lowest-energy state is obtained by filling up all ‘‘negative-energy’’ states (i.e., $E_k < 0$) with the WJ fermions. This filling creates a Fermi ‘‘surface’’ at the Fermi wave vectors $k_f = \pm\pi/2$. Δ in this case can be evaluated to be $\Delta = 1/\pi = 0.31831$, and the mean-field energy at $T=0$ is $E_{\text{MF}} = -0.4196J$ per site. The total energy is further lowered by fluctuations around the mean field. To second order, this lowering can be calculated by the standard formula

$$\Delta E = \sum_f \frac{|\langle 0 | (H - H_{\text{MF}}) | f \rangle|^2}{E_0 - E_f} , \quad (13)$$

where $|0\rangle$ and $|f\rangle$ are the ground state and the excited states of H_{MF} , respectively. The state $|f\rangle$ has two excited particles at wave vectors $k_1 + q$ and $k_2 - q$, and two holes at wave vectors k_1 and k_2 . Straightforward evaluation of Eq. (14) gives

$$\Delta E = -\frac{2J^2}{N^2} \sum_{k_1, k_2, q} \frac{\cos^2 q - \cos q \cos(k_1 - k_2 + q)}{E_{k_1+q} + E_{k_2-q} - E_{k_1} - E_{k_2}} , \quad (14)$$

where the prime in the summation means that the summation is restricted by the conditions $E_{k_1+q} > 0$, $E_{k_2-q} > 0$, $E_{k_1} < 0$, and $E_{k_2} < 0$. Numerical evaluation of Eq. (14) gives $\Delta E = -0.0155J$ per site. The total energy including the second-order correction at $T=0$ is therefore $E_{\text{tot}} = -0.4351J$ per site. This value is only 1.8% higher than the exact Bethe-ansatz value of $E = (\frac{1}{4} - \ln 2)J = -0.4431J$ per site.

The solution we described above has no long-range antiferromagnetic order since it is easy to show that $\langle d_i^\dagger d_i \rangle = \frac{1}{2}$ (recall that $\langle S_i^z \rangle = \langle d_i^\dagger d_i \rangle - \frac{1}{2}$). The excitation given by Eq. (11) near the Fermi surface is gapless in agreement with the Bethe-ansatz result. The energy spectrum near the Fermi surface is linear with velocity $v = (1 + 2\Delta)J = 1.6366J$, in quantitative agreement with the exact result obtained recently by Shastry²⁵ and Haldane²⁶ on the 1D Heisenberg model with $1/d^2$ interaction where Haldane finds²⁷ the velocity of the low-energy particles to be $(\pi/2)J = 1.5708J$. We also notice the resemblance between our energy spectrum in Eq. (11) and that of the 1D extended²⁸ resonating-valence-bond (RVB) state of Baskaran, Zou, and Anderson²⁹ (BZA). The resemblance can be further examined by dividing the 1D lattice into two sublattices and using the WJ transformation given in Eqs. (5)–(8). The mean-field, Δ , now is defined by $\Delta = \langle A_i B_{i+1} \rangle$, and the interactions between the A -type and B -type WJ fermions as seen from the Hamiltonian now becomes attractive. Thus, Δ can be viewed as the order parameter of the nearest-neighbor RVB state, and our solution discussed above describes a 1D gapless ‘‘superfluid’’ of the WJ fermions. Despite the resemblance, our solution and the RVB state of BZA are different in many aspects. For one, the particles in our solution are WJ fermions which are spinless, whereas the fermion objects in BZA’s RVB state are electron operators. While Δ describes the ‘‘bonding’’ of the nearest-neighbor WJ fermions, each WJ fermion involves many

spins in the system, and therefore Δ corresponds to more than nearest-neighbor spin bonds. The zero-temperature energy of our solution is also much lower than that of the RVB state of BZA, presumably because of the long-range “bonds” formed between the spins in our solution.

It is interesting to notice that, at mean-field level, a state with combined covalent bonding (Δ) and spin ordering ($\langle d_i^\dagger d_i \rangle = (1 \pm \Delta_2)/2$, where the $+$ sign is for one sublattice and the $-$ sign for another) has a lower mean-field energy ($-0.4322J$ per spin) than the covalent-bonding state we described above. This state breaks the translational symmetry, and the excitation spectrum has a gap of order $2\Delta_2 J$. The energy correction from second-order perturbation of this symmetry-broken state, however, is only $-0.0042J$ per spin because of the gapped spectrum in the energy denominator [cf., Eq. (15)], significantly smaller than that of the covalent-bonding state. The total energy including the second-order correction of this state is therefore nearly the same as that of the covalent-bonding state. We believe that higher-order corrections actually prefer the covalent-bonding state since similar energy denominators will also appear in the higher-order corrections.

IV. TWO-DIMENSIONAL AFM HEISENBERG MODEL IN A SQUARE LATTICE

With the 1D results in mind, we now study the 2D quantum AFM Heisenberg model in a square lattice. After substituting the WJ transformation into the Heisenberg Hamiltonian, we have

$$H = J \sum_{\langle ij \rangle} d_i^\dagger e^{i(\varphi_j - \varphi_i)} d_j + J \sum_{\langle ij \rangle} (d_i^\dagger d_i - \frac{1}{2})(d_j^\dagger d_j - \frac{1}{2}), \quad (15)$$

where the summations are over pairs of nearest neighbors. In contrast to the 1D case, the WJ phase factor, $e^{i(\varphi_j - \varphi_i)}$, now plays an important role in determining the energy spectrum. In the Appendix it is shown that the phase factor corresponds to that created by a gauge field with the vector potential given by

$$\mathbf{A}(\mathbf{r}_i) = \sum_{l \neq i} d_l^\dagger d_l \frac{\hat{\mathbf{z}} \times (\mathbf{r}_i - \mathbf{r}_l)}{(\mathbf{r}_i - \mathbf{r}_l)^2}. \quad (16)$$

This gauge potential generates long-range interactions between the WJ fermions, and clearly relates the 2D quantum spin problem to the anyon problem. In the mean-field treatment, which we adopt following Laughlin³⁰ and Mele,³¹ this vector potential corresponds to that of a uniform background gauge field (see the Appendix). The resulting Hamiltonian then describes a gas of WJ fermions moving in a uniform “magnetic” field and interacting via two-body potentials. It would be desirable to estimate the effect of fluctuations of the gauge field around the mean-field approximation. Unfortunately, this is quite difficult. Appropriate inclusion of the gauge-field fluctuation presents a major theoretical challenge to our method. It is nevertheless worthwhile to proceed the mean-field solution, and to find out whether the mean-

field solution presents an appropriate starting point. A somewhat different, but related, difficulty is also encountered in the conventional spin-wave approach based on the Holstein-Primakoff transformation. There the operator corresponding to the WJ phase factor is $\sqrt{1-n_i}\sqrt{1-n_j}$, where n_i is the number operator of Holstein-Primakoff bosons at site i . In the conventional spin-wave approach, it is assumed that the number of the bosons is small, and that the operators in the square roots are expandable as a power series of n_i (usually only the zeroth order is retained). For a three-dimensional system, this approximation is indeed justified, but for the 2D square lattice, the averaged boson occupation number is in the order of unity at any finite temperature even for a finite system with linear size ξ , where ξ is the spin correlation length (for an infinite 2D lattice, the averaged boson occupation number diverges logarithmically at any finite temperature).¹⁶

We consider the case where no true long-range AFM order is present, i.e., $\langle d_i^\dagger d_i \rangle = \frac{1}{2}$. This implies that the lattice size under consideration will be much larger than the spin correlation length. This case is most important at finite temperatures because it satisfies the Mermin-Wagner theorem. The vector potential in this case corresponds to that of a uniform magnetic field of half flux quanta per elementary plaquette. By choosing an appropriate gauge, the phase factor can be adsorbed by redefining a bond-dependent exchange parameter J_{ij} . In Fig. 1 we show the distribution of J_{ij} in one such gauge. Each heavy bond in the figure corresponds to a $J_{ij} = J e^{\pm i\pi}$, and each light bond to a $J_{ij} = J$. Following our discussion of the 1D AFM Heisenberg model, we define a bond-dependent mean field, Δ_{ij} , by

$$\Delta_{ij} = \Delta_1 e^{i\Theta_{ij}} = \langle d_i d_j^\dagger \rangle, \quad (17)$$

where i and j are nearest neighbors. The resulting mean-field Hamiltonian is

$$H_{\text{MF}} = \sum_{\langle ij \rangle} J_{ij} d_i^\dagger d_j + J \sum_{\langle ij \rangle} (2\Delta_{ij}) d_i^\dagger d_j + J \sum_{\langle ij \rangle} |\Delta_{ij}|^2. \quad (18)$$

It is easy to see that the phase Θ_{ij} , having the lowest en-

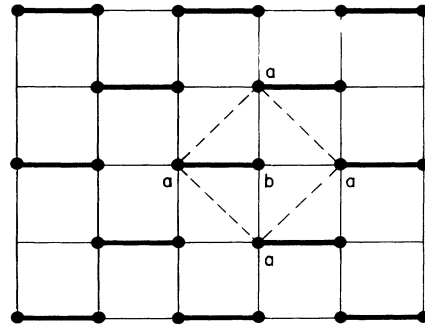


FIG. 1. The distribution of the phase factor in the gauge used in the text. Each heavy bond corresponds to a phase factor of $e^{i\pi}$, and each light bond to a phase factor 1. This distribution insures that each of the elementary plaquettes encloses a net flux of half quanta. The dashed lines indicate the primitive unit cell.

ergy, is the one equal to the averaged gauge phase, $\varphi_{ij} = \langle \varphi_j - \varphi_i \rangle$. Therefore, Θ_{ij} can be interpreted as being generated by the “gauge-field-induced” orbital currents which circulate around each elementary plaquette. The resulting state of Eq. (18) has been termed as the in-phase flux state.^{18,19}

Following the notation and the distribution of J_{ij} in Fig. 1, H_{MF} can be expressed in terms of the WJ fermion operators, a_i and b_j , of the two sublattices

$$H_{MF} = \frac{J}{2}(1 + 2\Delta_1) \times \sum_i [a_i^\dagger(b_{i-\tau_x} - b_{i+\tau_x} + b_{i+\tau_y} + b_{i-\tau_y}) + \text{H.c.}] + 2NJ\Delta_1^2, \quad (19)$$

where τ_x and τ_y are the vectors connecting two nearest neighbors. This Hamiltonian can be easily diagonalized and the energy spectrum of the in-phase flux state is

$$E_{\mathbf{k}}^\pm = \pm J(1 + 2\Delta_1) \sqrt{\sin^2 k_x + \cos^2 k_y}. \quad (20)$$

[Had we used the conventional asymmetric gauge, $\mathbf{A} = B\mathbf{y}\hat{x}$, $\sin k_x$ in Eq. (20) would be replaced by $\cos k_x$.] The advantage of using the gauge shown in Fig. 1 is that, in this gauge, the distribution of the phase factor has a unit cell equal to the magnetic unit cell. As in the 1D case, the negative-energy states of the spectrum are filled by the WJ fermions, whereas the positive-energy branch is empty in the $T \rightarrow 0$ limit. This filling self-consistently insures the absence of the long-range AFM order. The spectrum given in Eq. (20) obviously satisfies the two intrinsic properties of the WJ representation described in Sec. II.

The “bonding” amplitude, Δ_1 , can be calculated from its definition in Eq. (17),

$$\Delta_1 = \frac{1}{4N} \sum_{\mathbf{k}} \sqrt{\sin^2 k_x + \cos^2 k_y} [n_F(E_{\mathbf{k}}^-) - n_F(E_{\mathbf{k}}^+)]. \quad (21)$$

This gives $\Delta_1 = 0.2395$ in the $T \rightarrow 0$ limit. The temperature dependence of Δ_1 is shown in Fig. 2. Unlike the tem-

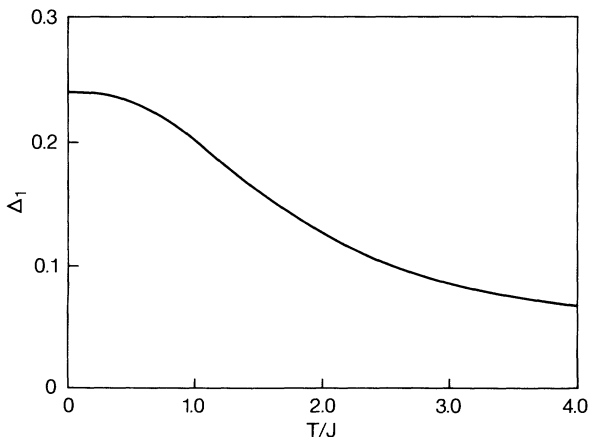


FIG. 2. The temperature dependence of the in-phase orbital current amplitude Δ_1 .

perature dependence of most mean fields, $\Delta_1(T)$ has no critical point at any finite temperature. This peculiar temperature dependence of Δ_1 reflects the fact that the in-phase flux state describes a paramagnetic state as the Mermin-Wagner theorem requires. It also indicates that fluctuations in the gauge field may not destroy our mean-field solution, since usually fluctuations have devastating effects only near the critical point.

The mean-field energy of the in-phase flux state in the $T \rightarrow 0$ limit is $E_{MF} = -0.297J$ per bond. The mean-field energy does not include the corrections from the virtual transitions between the lower and the upper band. The second-order correction from the S^z component alone can be calculated following the same procedure as that giving in the 1D case, and the energy of the in-phase flux state including this correction is $-0.324J$ per bond. There are corrections also from the fluctuations in the gauge fields. While the precise value of correction from the fluctuations in the gauge field is difficult to evaluate, it is clear from Eq. (15) that it is opposite to the corrections from the S^z component. The two, therefore, will partially cancel each other; hence, make the overall contribution from fluctuations relatively smaller. We believe that this partial cancellation makes our mean-field solution rather robust, as one could see from the predicted properties below.

The energy spectrum of the in-phase flux state as given in Eq. (20) is similar to that of the flux state discussed by Affleck and Marston.³² The two phases, however, are significantly different from each other in the sense that, in the case of the in-phase flux state, the “bonds” are formed between nearest-neighbor WJ fermions, whereas in the Affleck-Marston flux state, the “bonds” are formed between the Gutzwiller projected nearest-neighbor electrons.

We now calculate some properties of the in-phase flux state. In particular, we shall compare these properties with those of the linear spin-wave state since the two states are comparable in the approximation level, although their starting points are very different. The calculation of the spin Raman spectrum requires significant efforts, we therefore devote it to the next Section (V).

A. Single-particle excitation spectrum

As shown in Sec. II, reversing the direction of a single spin corresponds to adding (or subtracting) a WJ fermion from the system. Since the lower band of the in-phase flux state is filled, the single-particle excitation energy in the WJ fermion representation is $E_{WJ}(\mathbf{k}) = E_{\mathbf{k}}^+$. The energy spectrum given in Eq. (20) is for the particular gauge chosen in Fig. 1. In order to compare it with the spin-wave excitation spectrum, we uniformly shift all wave vectors by $(0, \pi/2)$. The WJ fermion excitation spectrum is, therefore, in the new gauge,

$$E_{WJ}(\mathbf{k}) = J(1 + 2\Delta_1) \sqrt{\sin^2 k_x + \sin^2 k_y}.$$

This is to be compared with the spin-wave spectrum

$$E_{SW}(\mathbf{k}) = 2J \sqrt{1 - \frac{1}{4}(\cos k_x + \cos k_y)^2}.$$

We first notice that the two spectra have identical \mathbf{k} dependences at small excitation energies, namely, that they all predict $E_{\mathbf{k}}$ to be linear in $|\mathbf{k}|$ for small $|\mathbf{k}|$. The velocities of the two spectra are also comparable, i.e., $v_{\text{WJ}} = 1.48J$ in the $T \rightarrow 0$ limit whereas $v_{\text{SW}} = 1.41J$. Since the two spectra are the result of mean-field or equivalent approximations, the velocities can be renormalized by high-order corrections. Second, the two spectra are identical along the $[11]$ ($k_x = k_y$) direction, $E_{\mathbf{k}} \approx \sin k_x$, apart from a slightly different prefactor. This \mathbf{k} dependence in the $[11]$ direction has been confirmed recently by neutron-scattering experiments.³³ The significant differences between the two spectra are near the zone edge point $(\pi, 0)$, at which the WJ fermion has a zero excitation energy, whereas the spin wave has $2J$. The energy spectrum of the WJ fermions along the $[10]$ direction, $E_{\mathbf{k}} = J(1 + 2\Delta)\sin k_x$, suggests that the spin excitations along this direction behave as those of the 1D chain [cf., Eq. (11)]. It would be interesting to see if this difference can be resolved by neutron-scattering experiments. The comparison of the two spectra is summarized in Fig. 3.

B. Specific heat

The internal energy, $U(T)$, of the in-phase flux state is

$$U(T) = \langle H \rangle = -2NJ\Delta_1(1 + \Delta_1).$$

The specific heat can be obtained by taking derivatives of $U(T)$ with respect to T . The result is shown in Fig. 4 by the solid curve. Also given in Fig. 4 are the numerical values of the specific heat of the Heisenberg model calculated from Monte Carlo methods.³⁴ The excellent agreement between the two is more than expected. More importantly, the in-phase flux state predicts a correct temperature dependence over the entire temperature range, namely a T^2 dependence at low temperature, a peak near $T/J = 0.6$, and a $1/T^2$ dependence at high temperature.

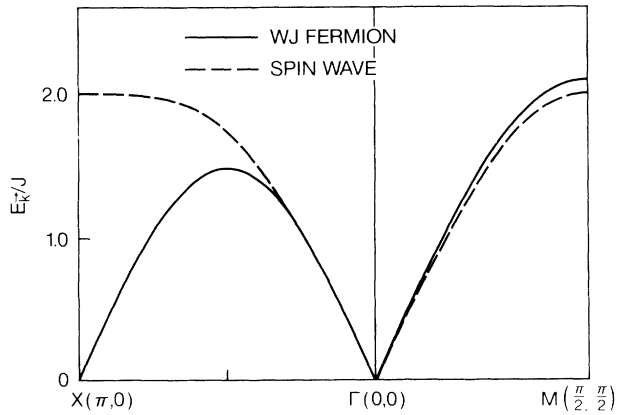


FIG. 3. Spectrum of single-particle excitation, i.e., excitation energy of reversing orientation of one spin in the system, predicted from the in-phase flux state of WJ fermions (solid curve) and that from spin-wave theories (dashed curve) along several symmetry directions.

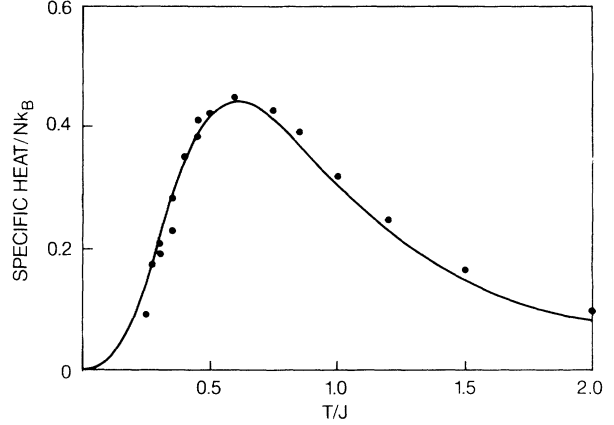


FIG. 4. Specific heat of the in-phase flux state of WJ fermions (solid curve). The solid circles are the numerical values of Ref. 34 calculated for the quantum Heisenberg model using the Monte Carlo method.

The correct T dependence at high temperature is a result of the fermionic nature of the excitations. While the spin-wave theory also predicts a T^2 dependence at low temperature, it neither predicts the peak near $T/J = 0.6$ nor the $1/T^2$ falling at high temperature.

V. RAMAN SPECTRUM OF THE 2D AFM HEISENBERG MODEL IN A SQUARE LATTICE

Besides the single spin excitation, there is another elementary excitation process in a quantum spin system, that is to flip two oppositely oriented spins simultaneously, leaving the total spin of the system unchanged. In the spin-wave approach, this process is described by creating two spin waves with opposite momentum, whereas in the in-phase flux state of the WJ fermions this process is described by exciting a WJ fermion from the lower (filled) band to the upper (empty) band. Raman-scattering experiments precisely measure such excitations, and are therefore imperative for understanding the dynamics of the quantum AFM Heisenberg model. Comparison of theoretical results with experimental spectra will be indicative of the nature of the excitations. Raman-scattering experiments⁴⁻⁷ on La_2CuO_4 and $\text{YBa}_2\text{Cu}_3\text{O}_{6+\delta}$ have revealed the very dynamical nature of the 2D spin- $\frac{1}{2}$ AFM Heisenberg system. The frequency shifts span a broad energy range from 1500 to 8000 cm^{-1} in La_2CuO_4 and from 1000 to 6000 cm^{-1} in $\text{YBa}_2\text{Cu}_3\text{O}_{6+\delta}$. It is also interesting to notice that the high-energy excitations have been shown to persist in the superconducting samples of $\text{YBa}_2\text{Cu}_3\text{O}_{6+\delta}$ and are highly correlated with the carrier density. In this section we calculate the Raman spectrum of the in-phase flux state of WJ fermions.

The Hamiltonian describing the interaction of light with pairs of spins is given by³⁵⁻³⁷

$$H_R = A \sum_{\langle ij \rangle} (\mathbf{E}_{\text{inc}} \cdot \boldsymbol{\sigma}_{ij})(\mathbf{E}_{\text{out}} \cdot \boldsymbol{\sigma}_{ij}) \mathbf{S}_i \cdot \mathbf{S}_j, \quad (22)$$

where \mathbf{E}_{inc} and \mathbf{E}_{out} are the electric fields of the incident

and scattered light, respectively, and σ_{ij} is the unit vector connecting nearest-neighbor spin sites i and j . To be more specific we consider the case where \mathbf{E}_{inc} is along the x' direction, and \mathbf{E}_{out} along the y' direction, where x' and y' are the axes along the diagonals of the square lattice. This configuration gives the B_{1g} symmetry as given in the literature.⁴⁻⁷ Substituting the WJ transformation into H_R , we obtain, for the B_{1g} spectra,

$$H_R = B \sum_i [d_i^\dagger (P_{i+\tau_y, i} d_{i+\tau_y} + P_{i-\tau_y, i} d_{i-\tau_y} - P_{i+\tau_x, i} d_{i+\tau_x} - P_{i-\tau_x, i} d_{i-\tau_x}) + (d_i^\dagger d_i - \frac{1}{2}) (d_{i+\tau_y}^\dagger d_{i+\tau_y} + d_{i-\tau_y}^\dagger d_{i-\tau_y} - d_{i+\tau_x}^\dagger d_{i+\tau_x} - d_{i-\tau_x}^\dagger d_{i-\tau_x})], \quad (23)$$

where $P_{i+\tau, i} = e^{i(\varphi_{i+\tau} - \varphi_i)}$ is the phase factor, and $B = AE_{\text{in}}E_{\text{out}}$. The phase factor is treated by the mean-field method described in the previous section. Using the notation in Fig. 1, we have

$$H_R \approx 2B \sum_{\mathbf{k}} [\varepsilon_{\mathbf{k}} e^{i\Theta_{\mathbf{k}}} a_{\mathbf{k}}^\dagger b_{\mathbf{k}} + \text{H.c.}] + \frac{4B}{N} \sum'_{\mathbf{k}, \mathbf{p}, \mathbf{q}} a_{\mathbf{k}+\mathbf{q}}^\dagger a_{\mathbf{k}} b_{\mathbf{p}-\mathbf{q}}^\dagger b_{\mathbf{p}} (\cos q_y - \cos q_x), \quad (24)$$

where $\varepsilon_{\mathbf{k}} = \sqrt{\sin^2 k_x + \cos^2 k_y}$, and $e^{i\Theta_{\mathbf{k}}} = (\cos k_y + i \sin k_x) / \varepsilon_{\mathbf{k}}$. The prime in the second summation means that the $\mathbf{q}=0$ term is excluded. Equation (24) indicates that H_R corresponds to light scattering by single and pair excitations of the spinless fermions from the lower subband, $E_{\mathbf{k}}^-$, to the upper subband, $E_{\mathbf{k}}^+$, or vice versa. We first consider the contribution from single interband excitations of the spinless fermions, since it is the dominant effect for not-too-high frequency shifts. The contribution from pair excitations will be discussed later. The effective Raman Hamiltonian for single interband excitation, H_{RS} , can be shown to be

$$H_{\text{RS}} = 2B(1 + 2\Delta_1) \sum_{\mathbf{k}} [a_{\mathbf{k}}^\dagger b_{\mathbf{k}} (\cos k_y + i \sin k_x) + b_{\mathbf{k}}^\dagger a_{\mathbf{k}} (\cos k_y - i \sin k_x)], \quad (25)$$

where we have used $\langle a_{\mathbf{k}}^\dagger a_{\mathbf{k}} \rangle = \langle b_{\mathbf{k}}^\dagger b_{\mathbf{k}} \rangle = \frac{1}{2}$, and

$$\langle a_{\mathbf{k}}^\dagger b_{\mathbf{k}} \rangle = -\frac{1}{2} e^{i\Theta_{\mathbf{k}}} \tanh(E_{\mathbf{k}} / 2k_B T),$$

which are the basic properties of the in-phase flux state.

The extinction coefficient³⁵ of the Raman scattering is proportional to the correlation function, $R(\omega)$,

$$R(\omega) = \text{Im} \langle \langle H_R | H_R \rangle \rangle_{\omega + i\delta}, \quad (26)$$

where ω is the frequency shift in the Raman scattering, and $\langle \langle H_R | H_R \rangle \rangle_{\omega + i\delta}$ is the Fourier transformation of the correlation function,

$$U(t, t') = -\Theta(t - t') \langle [H_R(t), H_R(t')] \rangle.$$

In order to obtain the Raman spectrum contributed from

single interband excitations, $R_s(\omega)$, we first define the following Green's functions:

$$G_{\mathbf{k}}(t, t') = -i\Theta(t - t') \langle [b_{\mathbf{k}}^\dagger(t) a_{\mathbf{k}}(t), H_R(t')] \rangle, \quad (27)$$

$$F_{\mathbf{k}}(t, t') = -i\Theta(t - t') \langle [a_{\mathbf{k}}^\dagger(t) b_{\mathbf{k}}(t), H_R(t')] \rangle, \quad (28)$$

$$I_{b\mathbf{k}}(t, t') = -i\Theta(t - t') \langle [b_{\mathbf{k}}^\dagger(t) b_{\mathbf{k}}(t), H_R(t')] \rangle, \quad (29)$$

and

$$I_{a\mathbf{k}}(t, t') = -i\Theta(t - t') \langle [a_{\mathbf{k}}^\dagger(t) a_{\mathbf{k}}(t), H_R(t')] \rangle. \quad (30)$$

The equations of motion of these Green's functions can be established using Zubarev's method.³⁸

The Hamiltonian of the spin system is defined in Eq. (15). While the phase factor in Eq. (15) is approximated as a uniform gauge field as discussed in the above section, we shall retain the interaction between the WJ fermions as given by the second term in Eq. (15) in establishing the equation of motion of the above Green's functions. The spin Hamiltonian is most conveniently expressed in the momentum space,

$$H \approx J \sum_{\mathbf{k}} [\varepsilon_{\mathbf{k}} e^{-i\Theta_{\mathbf{k}}} a_{\mathbf{k}}^\dagger b_{\mathbf{k}} + \text{H.c.}] + \frac{2J}{N} \sum'_{\mathbf{k}, \mathbf{p}, \mathbf{q}} X(\mathbf{q}) a_{\mathbf{k}+\mathbf{q}}^\dagger a_{\mathbf{k}} b_{\mathbf{p}-\mathbf{q}}^\dagger b_{\mathbf{p}}, \quad (31)$$

where $X(\mathbf{q}) = \cos q_x + \cos q_y$. The interaction between the WJ fermions manifests itself in the higher-order Green's functions. For example, we have

$$\begin{aligned} \omega G_{\mathbf{k}}(\omega) &= J \varepsilon_{\mathbf{k}} e^{-i\Theta_{\mathbf{k}}} [I_{b\mathbf{k}}(\omega) - I_{a\mathbf{k}}(\omega)] \\ &+ \frac{2J}{N} \sum'_{\mathbf{p}, \mathbf{q}} X(\mathbf{q}) [\langle \langle b_{\mathbf{k}-\mathbf{q}}^\dagger a_{\mathbf{k}-\mathbf{q}} b_{\mathbf{p}-\mathbf{q}}^\dagger b_{\mathbf{p}} | H_R \rangle \rangle_{\omega} \\ &- \langle \langle a_{\mathbf{p}+\mathbf{q}}^\dagger a_{\mathbf{p}} b_{\mathbf{k}-\mathbf{q}}^\dagger a_{\mathbf{k}} | H_R \rangle \rangle_{\omega}]. \end{aligned} \quad (32)$$

We next truncate the higher-order Green's function to get a set of integral equations. The method used is reminiscent of the self-consistent random-phase approximation (RPA). Thus, for example,

$$\begin{aligned} \langle \langle b_{\mathbf{k}-\mathbf{q}}^\dagger a_{\mathbf{k}-\mathbf{q}} b_{\mathbf{p}-\mathbf{q}}^\dagger b_{\mathbf{p}} | H_R \rangle \rangle_{\omega} &\approx \delta_{\mathbf{k}\mathbf{p}} [\langle a_{\mathbf{k}-\mathbf{q}} b_{\mathbf{p}-\mathbf{q}}^\dagger \rangle I_{b\mathbf{k}}(\omega) \\ &- \langle b_{\mathbf{k}}^\dagger b_{\mathbf{p}} \rangle G_{\mathbf{k}-\mathbf{q}}(\omega)]. \end{aligned} \quad (33)$$

Using the relation

$$\frac{2}{N} \sum_{\mathbf{q}} X(\mathbf{q}) \langle a_{\mathbf{k}-\mathbf{q}} b_{\mathbf{k}-\mathbf{q}}^\dagger \rangle = 2\Delta_1 \varepsilon_{\mathbf{k}} e^{-i\Theta_{\mathbf{k}}}, \quad (34)$$

we obtain

$$\omega G_{\mathbf{k}}(\omega) = E_{\mathbf{k}}^+ e^{-i\Theta_{\mathbf{k}}} [I_{b\mathbf{k}}(\omega) - I_{a\mathbf{k}}(\omega)] . \quad (35)$$

Similar manipulation gives

$$F_{\mathbf{k}}(\omega) = -e^{2i\Theta_{\mathbf{k}}} G_{\mathbf{k}}(\omega) , \quad (36)$$

$$\begin{aligned} \omega I_{b\mathbf{k}}(\omega) = & B(1+2\Delta_1) \epsilon_{\mathbf{k}} (e^{2i\Theta_{\mathbf{k}}} - e^{-2i\Theta_{\mathbf{k}}}) \tanh(E_{\mathbf{k}}^+ / 2k_B T) \\ & + 2E_{\mathbf{k}}^+ e^{i\Theta_{\mathbf{k}}} G_{\mathbf{k}}(\omega) - Q_{\mathbf{k}}(\omega) \tanh(E_{\mathbf{k}}^+ / 2k_B T) , \end{aligned} \quad (37)$$

and

$$I_{a\mathbf{k}}(\omega) = -I_{b\mathbf{k}}(\omega) , \quad (38)$$

where

$$Q_{\mathbf{k}}(\omega) = \frac{J}{N} \sum_{\mathbf{q}} X(\mathbf{k}-\mathbf{q}) (e^{i\Theta_{\mathbf{k}}} + e^{-i\Theta_{\mathbf{k}}} e^{2i\Theta_{\mathbf{q}}}) G_{\mathbf{q}}(\omega) . \quad (39)$$

This set of integral equations can be solved exactly by postulating that

$$\frac{J}{N} \sum_{\mathbf{q}} X(\mathbf{k}-\mathbf{q}) G_{\mathbf{q}}(\omega) = \epsilon_{\mathbf{k}} e^{i\Theta_{\mathbf{k}}} f(\omega) \quad (40a)$$

and

$$\frac{J}{N} \sum_{\mathbf{q}} X(\mathbf{k}-\mathbf{q}) G_{\mathbf{q}}(\omega) e^{2i\Theta_{\mathbf{q}}} = -\epsilon_{\mathbf{k}} e^{-i\Theta_{\mathbf{k}}} f(\omega) , \quad (40b)$$

and solve for $f(\omega)$ self-consistently. The contribution from the single interband excitations, $R_s(\omega)$, can be obtained from $G_{\mathbf{k}}(\omega)$ and $F_{\mathbf{k}}(\omega)$ by proper summation over \mathbf{k} , as can be easily seen from its definition. The final result is

$$R_s(\omega) = 4B^2(1+2\Delta_1)^2 \text{Im} \left[\frac{\chi(\omega + i\delta)}{1 + \chi(\omega + i\delta)} \right] , \quad (41)$$

where

$$\chi(\omega) = \frac{J}{N} \sum_{\mathbf{k}} \frac{8E_{\mathbf{k}}^+ \cos^2 k_y \sin^2 k_x}{\epsilon_{\mathbf{k}}^2(\omega^2 - 4E_{\mathbf{k}}^+{}^2)} \tanh(E_{\mathbf{k}}^+ / 2k_B T) . \quad (42)$$

The weighting factor in $\chi(\omega)$ favors excitations at the band edge, and suppresses excitations at the band center ($E_{\mathbf{k}}^{\pm} \sim 0$), confirming the fact that Raman-scattering experiments are not sensitive to long-wavelength excitations. It is also interesting to note that Raman-scattering does not simply measure the density of states of the excitations. For example, the density of states of the excitations has a Van Hove singularity at $\omega = 2J(1+2\Delta_1)$, which, however, is cancelled in Eq. (42) by the weighting factor. The denominator, $1 + \chi(\omega)$, in Eq. (41) comes from the interaction between the spinless fermions, i.e., the second term of Eq. (31). Since $\text{Im}\chi(\omega + i\delta)$ is largest at the band edge, it is obvious that the interaction between the spinless fermions (or quantum fluctuations) is very important for the Raman spectrum to peak at a value below the band edge excitation. In fact, the peak position of the Raman spectrum is determined by the vanishing of the real part of $1 + \chi(\omega)$.

The calculated spectrum is compared with the experi-

mental Raman scattering intensity of La_2CuO_4 , as shown in Fig. 5. Below the frequency shift of about 4000 cm^{-1} , our calculation agrees very well with the experimental data. The calculated spectrum shape depends only on the parameter $\alpha = J(1+2\Delta_1)$, which we obtain from the comparison to be 1568 cm^{-1} . For such a large value of α , Δ_1 hardly changes between zero temperature and room temperature. For example, Δ_1 is calculated from Eq. (21) to be 0.2365 at $T = 300 \text{ K}$. The exchange energy, J , thus can be determined using the zero temperature value of Δ_1 to be 1060 cm^{-1} . This value of J agrees remarkably well with the previous estimated value from the light scattering spectrum⁶ and from analyzing^{8,39,40} the neutron-scattering data.¹⁻³ The fact that the exchange parameter, J , obtained from the Raman-scattering and the neutron-scattering data agrees with each other is significant, since neutron scattering measures the long-wavelength excitations. Because of the large value of J , our theory predicts very little change in the Raman-scattering spectrum between zero temperature and room temperature, which is indeed experimentally observed. We have also calculated the extinction coefficient for the case where \mathbf{E}_{inc} and \mathbf{E}_{out} are both along the Cu-O bond (the xx or yy spectrum), and find that it is the same expression as that given in Eqs. (41) and (42). That the xx (or yy) and the $x'y'$ spectra are the same can be proven exactly from the symmetry consideration of Eq. (22), assuming that the interaction of light with pairs of nearest-neighbor spins described by Eq. (22) is the only interaction. Our theory preserves this symmetry. (The diagonal-next-neighbor spin pair scatterings may give rise to the A_{1g} and B_{2g} spectra.⁶ The experimental xx component then contains the A_{1g} and the B_{1g} spectra.)

Since Eq. (41) only includes single interband spinless

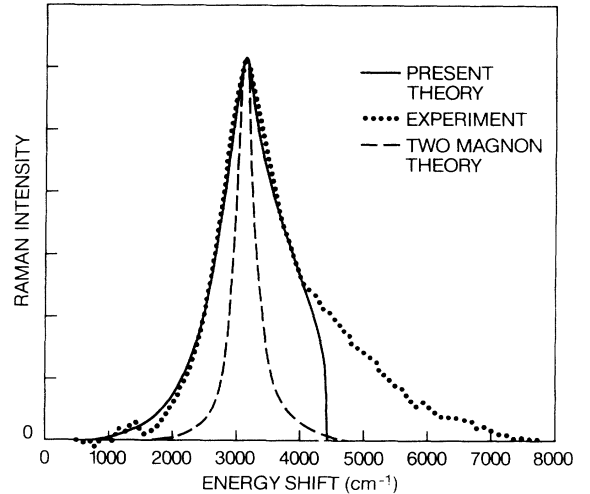


FIG. 5. Comparison of the theoretical Raman spectrum contributed from single interband excitations of WJ fermions, i.e., Eq. (41) (solid curve), with the experimental data of La_2CuO_4 (dotted curve). The experimental curve is from Ref. 6 for which all instrumental responses have been corrected. The dashed curve is calculated from the spin-wave theory of Parkinson (Ref. 36).

fermion excitations, the maximum frequency shift it predicts is $2\sqrt{2}J(1+2\Delta_1)$, or 4434 cm^{-1} for La_2CuO_4 . The experimental spectrum shape has a long tail extending up to about 8000 cm^{-1} , approximately twice the maximum frequency shift predicted from single spinless fermion excitations, suggesting that the pair excitations of the spinless fermions are important at large frequency shifts.

The evaluation of the Raman intensity contributed from the pair excitation of the spinless fermions is very complicated. We shall simplify it by using the mean-field Hamiltonian for the spin system, i.e., Eq. (19). This is tantamount to neglecting fluctuations around the in-phase flux state. While the fluctuations are expected to be important for determining the shape of the spectra, as we have seen in the evaluation of $R_s(\omega)$, we expect the resulting order of magnitude of the pair contribution relative to the single contribution to be correct. When the approximation is adopted, the evaluation is most conveniently done in the representation which diagonalizes the mean-field Hamiltonian. By using the transformation, $a_k = (C_k + e^{-i\Theta_k} D_k)/\sqrt{2}$, and $b_k = (D_k - e^{i\Theta_k} C_k)/\sqrt{2}$, Eq. (19) becomes

$$H_{\text{MF}} = \sum_k (D_k^\dagger D_k - C_k^\dagger C_k) E_k^+ . \quad (43)$$

$$R_2(\omega) = \frac{4\pi JB^2}{N^3} \sum_{k,p,q} [\cos^2 q_x (1 + e^{i(\Theta_{k+q} + \Theta_p - \Theta_{p-q} - \Theta_k)}) - 2 \cos q_x \cos(k_x + q_x - p_x) e^{i(\Theta_p - \Theta_k)}] \delta(\omega - E_{k+q}^+ - E_{p-q}^+ - E_k^+ - E_p^+) , \quad (45)$$

for $\omega > 0$ and at $T=0$. Obviously Eq. (45) extends the Raman frequency shift up to $4\sqrt{2}J(1+2\Delta_1)$. It is computationally difficult to handle Eq. (45) because of the six-dimensional integral implied in the summation. We shall further simplify $R_2(\omega)$ by setting $q=0$ in the δ -function argument, corresponding to approximating all pair excitation processes as vertical in the energy diagram, and $\Theta_{k+q} - \Theta_k \approx q \cdot \nabla \Theta_k$. These approximations allow the summation of q to be done analytically. For $\omega \ll 2J(1+2\Delta_1)$ we find

$$R_2(\omega) \approx (8/3\pi^3) B^2 [\omega/2J(1+2\Delta_1)]^3 / (1+2\Delta_1) .$$

This is compared with the similar result for $R_s(\omega)$ in Eq. (41) at the same frequency region,

$$R_s(\omega) = (1+2\Delta_1)^2 B^2 [\omega/2J(1+2\Delta_1)]^3 / (1+2\Delta_1) .$$

This gives $R_2(\omega)/R_s(\omega) = 0.04$. Therefore, as expected, the interband pair excitations are not important at small frequencies. The calculated Raman spectrum, $R(\omega) = R_s(\omega) + R_2(\omega)$, is shown in Fig. 6. As can be seen, $R(\omega)$ reasonably accounts for the asymmetrical shape of the experimental spectrum, and $R_2(\omega)$ has the correct order of magnitude compared with the intensity at the tail of the experimental spectrum. The sharp separation at the single-particle band edge, i.e., near 4400

The pair excitation term in the Raman-scattering Hamiltonian, i.e., the second term in Eq. (24), also needs to be transformed. This creates 16 different terms corresponding to various ways of exciting the pairs. Many of them have a one interband and one intraband excitation, and therefore in the region $\omega < 2\sqrt{2}J(1+2\Delta_1)$ they can be considered as effective single-particle excitations. These pair excitations contributed the factor $(1+2\Delta_1)$ in Eq. (6). In addition to these pair excitations, there are two terms corresponding to interband pair excitations, and they cannot be considered as effectively single excitations over the entire frequency region. More explicitly, the pair excitation part of the Raman Hamiltonian, i.e., the second term of Eq. (24), is

$$H_{\text{RP}} = \frac{B}{N} \sum'_{k,p,q} [e^{i(\Theta_{k+q} + \Theta_p)} D_{k+q}^\dagger D_{p-q}^\dagger C_k C_p + \text{H.c.}] \times (\cos q_y - \cos q_x) + \text{other terms} . \quad (44)$$

In the mean-field approximation, the "other terms" in Eq. (44) are effectively single excitations, and their contributions have been taken into account in $R_s(\omega)$. The pair excitation contribution to the Raman intensity, $R_2(\omega)$, can be obtained by establishing the equation of motion for H_{RP} . Using Eq. (43), we obtain

cm^{-1} , is caused by the different approximations used for calculating the single interband excitation and pair excitation contributions.

The experimental Raman spectrum has been previous-

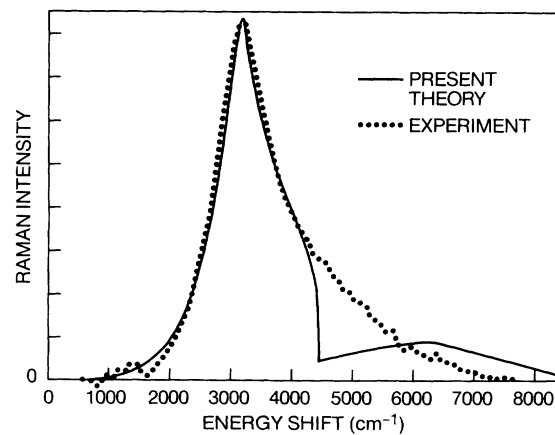


FIG. 6. The theoretical Raman spectrum including both single excitations [Eq. (41)] and pair excitations [Eq. (45)] of WJ fermions. The sharp separation near the single excitation band edge ($\sim 4400 \text{ cm}^{-1}$) is caused by the different approximations used in deriving the two contributions (see the text).

ly interpreted in terms of two-magnon (spin-wave) scattering theory of Elliott and Thorpe,³⁵ and of Parkinson,³⁶ and has also been analyzed using perturbation theory around the Ising limit.⁶ The two magnon theory is expected to be valid for classical spins ($S \geq 1$), and its applicability to quantum spins is questionable, as mentioned in the Introduction. The prediction of the spectrum shape of the two-magnon theory is shown in Fig. 5 by the dashed line. The width of the spectrum predicted by the two-magnon theory is too small compared with that of the experimental data. The apparent improvement of the present theory over the two-magnon theory indicates the importance of the quantum nature of the spin- $\frac{1}{2}$ system. The analysis⁶ of Singh *et al.* using the Ising-limit perturbation theory gives good agreement between the calculated frequency moments and the experimental ones, and their calculation also concludes that the quantum fluctuations are very important for the 2D spin- $\frac{1}{2}$ Heisenberg antiferromagnet. A direct comparison of the present theory with their calculation is difficult since the spectrum shape is not calculated in their analysis. The Raman spectrum has also been discussed by Hsu⁴¹ in the context of the generalized Affleck-Marston flux state. In his treatment, the excitations are projected spin waves which cannot be simply expressed as spin operators and therefore explicit calculation of the Raman spectrum cannot be done. Our treatment of transforming spin operators into Wigner-Jordan fermions offers distinct advantages for calculating the spectra.

VI. SUMMARY AND DISCUSSION

The advantage of using the WJ spinless fermion representation in studying low-dimensional quantum antiferromagnetism is that it automatically preserves the spin-commutation relations, as well as the spin on-site exclusion principle. We have shown that the 1D $S=\frac{1}{2}$ AFM Heisenberg model can be viewed as a 1D liquid of WJ fermions. A mean-field theory, corresponding to the covalent-bonding state of WJ spinless fermions, is found in quantitative agreement with the exact results from the Bethe-ansatz solution. The mean-field state has no long-range AFM order, the zero-temperature energy including second-order correction is $-0.4351J$ per site, compared with the exact value of $-0.4431J$ per site, and the excitation spectra is gapless and linear in momentum at low energies. The velocity of the particles near the Fermi surface is $1.6366J$, compared with $1.5708J$ obtained by Haldane for the $1/d^2$ -interaction Heisenberg model. The method used for studying the 1D model is applied to the 2D quantum AFM Heisenberg model in a square lattice. The resulting state at finite temperature is the in-phase flux state. This state satisfies the Mermin-Wagner theorem; i.e., it does not have a long-range AFM order at finite temperatures. The dispersion of the single-particle excitation spectrum of the in-phase flux state is similar overall to that of spin waves with significant differences near the edge point $(\pi, 0)$ of the Brillouin zone. The specific heat of the in-phase flux state has a correct tem-

perature dependence over the entire temperature range, namely, a T^2 dependence at low temperature, a peak near $T/J=0.6$, and a $1/T^2$ decreasing at high temperature. In contrast, the spin-wave theory only correctly predicts the T^2 dependence at low temperature. The Raman spectrum of the in-phase flux state is calculated and found that it significantly improves the Raman spectrum of spin-wave theories compared with the experimental spectrum of La_2CuO_4 , suggesting that the short-wavelength excitations of the quantum AFM Heisenberg model can be well described by that from the in-phase flux state. The exchange parameter, J , obtained from the comparison of the experimental spectra with the theoretical calculation is 1060 cm^{-1} , agrees remarkably well with that evaluated from analyzing neutron-scattering experimental data. These evidences suggest that the in-phase flux state of WJ fermions corresponds very closely to the true eigenstate of the quantum Heisenberg model in a square lattice.

Our calculation indicates the vital importance of the spin correlation in the spin- $\frac{1}{2}$ AFM Heisenberg system. A spinless fermion at site j represents a vortexlike spin excitation with the “vortex core” at site j and all the spins at other sites circulating around it. Thus, reversal of the spin direction at any site necessary involves corresponding changes of the whole spin system. We particularly notice that the excitations in our treatment are fermionic. This fermionic statistics reflects the phase change in the many-spin-wave function when a spin in the system reverses its orientation. Whether the difference in the statistics of the excitations, fermionic in our approach and bosonic in the spin-wave approach, is significant is not clear theoretically, since the statistics of 2D interacting particles tends to be obscure. Nevertheless, it would be interesting to see whether the difference could be resolved experimentally.

ACKNOWLEDGMENTS

The author is grateful to M. J. Rice and T. E. Orlowski for their encouragement and discussions.

APPENDIX

In this appendix, we show that the phase factor in Eq. (15) is that of the vector potential in Eq. (16), and that in the mean-field approximation and in the continuum limit the vector potential corresponds to that of a uniform magnetic field. Equation (16) is obtained by writing the phase difference between site j and site i in the following form:

$$\varphi_j - \varphi_i = \int_i^j d\mathbf{r} \cdot \nabla \varphi(\mathbf{r}), \quad (\text{A1})$$

and taking the derivative of φ_i with respect to \mathbf{r}_i . In the mean-field approximation, $d_l^\dagger d_l$ is uniform and therefore can be taken out from the summation in Eq. (16). The summation over l in Eq. (16) is done in the continuum

limit. In this limit, we can replace $\sum_{l \neq 1}$ by $A^{-1} \int dx dy$, where A is the area of an elementary plaquette. The integral is bounded by a square of linear dimension a , and we will take the limit $a \rightarrow \infty$ at the end of integration. Without loss of generality, we assume $\mathbf{r}_i = x_i \hat{x}$. After integration over dx , we obtain

$$\nabla_{\mathbf{r}_i} \varphi(\mathbf{r}_i) = -\frac{n}{2A} \hat{z} \times \hat{x} \int_{-a/2}^{a/2} dy \ln \frac{(a/2 - x_i)^2 + y^2}{(a/2 + x_i)^2 + y^2}, \quad (\text{A2})$$

where $n = \langle d_l^\dagger d_l \rangle$. The argument within the log is now expanded as a power series of $x_i / [(a/2)^2 + y^2]$, and we only need to retain the first order. The integration over dy can be easily done. Generalizing to arbitrary \mathbf{r}_i , we have

$$\nabla_{\mathbf{r}_i} \varphi(\mathbf{r}_i) = \frac{2\pi}{\Phi_0} \frac{1}{2} \mathbf{B} \times \mathbf{r}_i, \quad (\text{A3})$$

where Φ_0 is the unit flux quantum, and $\mathbf{B} = (n/A) \Phi_0 \hat{z}$ is the uniform gauge field. In the in-phase flux state, $n = \frac{1}{2}$, \mathbf{B} then represents a self-generated uniform gauge field of strength half flux quanta per elementary plaquette.

-
- ¹K. Yamada *et al.*, Phys. Rev. B **40**, 4557 (1989).
²G. Shirane *et al.*, Phys. Rev. Lett. **59**, 1613 (1987); R. J. Birgeneau *et al.*, Phys. Rev. B **38**, 6614 (1988); M. A. Kastner *et al.*, *ibid.* **38**, 6636 (1988).
³D. Vaknin *et al.*, Phys. Rev. Lett. **58**, 2808 (1987).
⁴K. B. Lyons, P. A. Fleury, J. P. Remeika, A. S. Cooper, and T. J. Negran, Phys. Rev. B **37**, 2353 (1988).
⁵K. B. Lyons, P. A. Fleury, L. F. Schneemeyer, and J. V. Waszczak, Phys. Rev. Lett. **60**, 732 (1988).
⁶R. R. P. Singh, P. A. Fleury, K. B. Lyons, and P. E. Sulewski, Phys. Rev. Lett. **62**, 2736 (1989).
⁷K. B. Lyons, P. E. Sulewski, P. A. Fleury, H. L. Carter, A. S. Cooper, and G. P. Espinosa, Z. Fisk, and S. W. Cheong, Phys. Rev. B **39**, 9693 (1989).
⁸S. Chakravarty, B. I. Halperin, and D. Nelson, Phys. Rev. Lett. **60**, 1057 (1988); Phys. Rev. B **39**, 2344 (1989).
⁹H. Bethe, Z. Phys. **71**, 205 (1931); L. Hulthen, Ark. Mat. Astron. Fyz. **26A** (1938).
¹⁰E. H. Lieb and F. Y. Wu, Phys. Rev. Lett. **20**, 1445 (1968).
¹¹See, for example, W. Jones and N. H. March, *Theoretical Solid State Physics* (Dover, New York, 1973), Chap. 4.
¹²See, for example, R. R. P. Singh, Phys. Rev. B **39**, 9760 (1989).
¹³A. V. Chubukov, J. Phys. (Paris) **45**, 401 (1984).
¹⁴See, for example, D. A. Huse and V. Elser, Phys. Rev. Lett. **60**, 2531 (1988).
¹⁵N. D. Mermin and H. Wagner, Phys. Rev. Lett. **17**, 1133 (1966).
¹⁶Y. R. Wang and M. J. Rice, Phys. Rev. B **45**, 5045 (1992).
¹⁷T. Holstein and H. Primakoff, Phys. Rev. **58**, 1098 (1940).
¹⁸Y. R. Wang, Phys. Rev. B **43**, 3786 (1991).
¹⁹Y. R. Wang, Phys. Rev. B **43**, 13 774 (1991).
²⁰P. Jordan and E. Wigner, Z. Phys. **47**, 631 (1928).
²¹J. Ambjorn and G. Semenoff, Phys. Lett. B **226**, 107 (1989).
²²E. Fradkin, Phys. Rev. Lett. **63**, 322 (1989).
²³E. J. Mele, Phys. Scr. T **27**, 82 (1989).
²⁴G. D. Mahan, *Many-Particle Physics* (Plenum, New York, 1981), p. 49.
²⁵B. S. Shastry, Phys. Rev. Lett. **60**, 639 (1988).
²⁶F. D. M. Haldane, Phys. Rev. Lett. **60**, 635 (1988).
²⁷F. D. M. Haldane, Phys. Rev. Lett. **66**, 1529 (1991).
²⁸P. W. Anderson, Int. J. Mod. Phys. B **4**, 181 (1990).
²⁹G. Baskaran, Z. Zou, and P. W. Anderson, Solid State Commun. **63**, 973 (1987).
³⁰V. Kalmeyer and R. B. Laughlin, Phys. Rev. Lett. **59**, 2095 (1987).
³¹E. J. Mele, Phys. Rev. B **40**, 2670 (1989).
³²I. Affleck and J. B. Marston, Phys. Rev. B **37**, 3774 (1988); G. Kotliar, *ibid.* **37**, 3664 (1988).
³³S. M. Hayden *et al.*, Phys. Rev. Lett. **67**, 3622 (1991), and references therein.
³⁴M. S. Makivic and H. Q. Ding, Phys. Rev. B **43**, 3562 (1991).
³⁵R. J. Elliott and M. F. Thorpe, J. Phys. C **2**, 1630 (1969).
³⁶J. B. Parkinson, J. Phys. C **2**, 2012 (1969).
³⁷B. S. Shastry and B. I. Shraiman, Phys. Rev. Lett. **65**, 1068 (1990).
³⁸D. N. Zubarev, Usp. Fiz. Nauk **71**, 71 (1960) [Sov. Phys. Usp. **3**, 320 (1960)].
³⁹A. Auerbach and D. P. Arovas, Phys. Rev. Lett. **61**, 617 (1988).
⁴⁰H.-Q. Ding and M. S. Makivic, Phys. Rev. Lett. **64**, 1449 (1990).
⁴¹T. C. Hsu, Phys. Rev. B **41**, 11 379 (1990).